Determination of *g*-factor for Free Radicals in *dpph* using Electron Spin Resonance

Matthew Brown

Condensed Matter
Laboratory Project

School of Physics and Astronomy
University of Birmingham
November 2023

Abstract

Electron spin resonance (ESR) has been employed to determine the Landé g-factor for free radicals in *dpph* and their spin-spin relaxation times at room temperature and at 243 K with the use of freezing agent. A Robinson oscillator was used to oscillate a tank circuit at a nominal 50 MHz and to record signal losses to identify ESR. A modulating field was used to obtain the first derivative ESR lines with greater resolution than the true absorption lines. This signal was retrieved from a lock-in amplifier whose parameters were optimised for the clearest ESR line. Under nominal conditions, the g-factor was found to be 2.091 ± 0.081 with spin-spin relaxation time, T_2, equal to 0.050 ± 0.002 μs, in good agreement with literature values. The B-field of the field coil was shown to behave differently to theory, leading to artificially fluctuant g values at different positions inside the coil. The tank circuit oscillation was varied, with a consistent g-factor observed, but slight variation in T_2, though a conclusive dependence was not achievable. A clear dependence of T_2 on temperature was observed, with a shorter relaxation time for lower temperatures.

Keywords: Electron Spin Resonance, g-factor, *dpph*, line width, spin-spin relaxation.

1 Introduction

Alfred Landé was the first to describe the g-factor for the electron, the parameter that characterises the magnetic moment and angular momentum of a particle, and is subsequently referred to as the Landé g-factor [1]. It's theoretical value is $g = 2$, however, it has been shown to deviate slightly due to considerations from quantum electrodynamics [2]. Since this factor is characteristic of a given material, one can characterise unknown materials in a sample by finding the g-value, hence its use in a range of fields including MRI scanning. This investigation focuses on inducing electron spin resonance (ESR) through the use of microwave frequencies to drive oscillations of a tank circuit to evaluate the Landé g-factor experimentally of free radicals in a sample of *dpph*. The line width of the ESR signal is also investigated along with its relation to relaxation time for different tank circuit microwave frequencies, and temperature.

2 Theory of Electron Spin Resonance

Electrons may be in spin-up or spin-down states, and have quantum spin number, $s = \frac{1}{2}$ with magnetic components $m_s = \pm\frac{1}{2}$. In the absence of a magnetic field, the alignments of unpaired electron spins in a given sample will be random, all of equal energy, the zero-field energy [3]. Once a magnetic field is applied, each electron must align itself either spin-up, or spin-down, parallel or antiparallel to the field, due to its spin-half quantum number. If aligned parallel to the field, the energy of the state will be $\frac{1}{2}g\mu_B B$ less than the zero-field energy, and $\frac{1}{2}g\mu_B B$ more than the zero-field energy if antiparallel, where μ_B is the Bohr Magneton. This splitting of states is the Zeeman splitting of energy levels. Therefore the energy separation of the two states is $g\mu_B B$ and this increases linearly with an increasing magnetic field. If electromagnetic radiation of frequency ν is applied to the sample, each electron may transition from the lower energy state to the higher energy state by absorbing energy, provided,

$$h\nu = g\mu_B B. \tag{1}$$

This is known as the resonance condition, and if met, the phenomenon of electron spin resonance (ESR) is observed. At the same time electrons aligned parallel to the field absorb energy, electrons that are antiparallel will be stimulated and emit energy of $h\nu$ and align

themselves parallel to the magnetic field. Knowing the resonance condition allows for the determination of the resonant magnetic field, B_0, which subsequently can be used to evaluate the g-factor for free electrons experimentally. Additionally, the half-width, ΔB, or the relaxation time can be deduced from,

$$\Delta E = \frac{h\nu}{B}\Delta B, \tag{2}$$

where ΔB is the distance measured from the absorption spectral line's centre to the point of half the absorption at resonance.

The absorption of this energy relies on more electrons in the lower spin state, which at room temperature is marginal. This can be shown by considering the Maxwell-Boltzmann distribution, where the ratio of the number of electrons in the higher spin state, N_{upper}, to the number in the lower state, N_{lower}, is given by

$$\frac{N_{upper}}{N_{lower}} = \exp\left(-\frac{E_{upper} - E_{lower}}{k_B T}\right). \tag{3}$$

This investigation uses radio frequencies around 50 MHz to drive oscillations of a tank circuit at room temperature. Substituting this frequency in $h\nu$ for $E_{upper} - E_{lower}$ in equation 3, one finds the ratio of electrons in the upper state to lower state to be 0.99999, essentially unity. This illustrates that at room temperature, the number of electrons in the upper and lower states are almost equal. As a result, the absorption signal is extremely small, comparable to electronic noise, and hence some ingenuity is needed to extract this signal.

3 Experimental Set-up

Figure 3.1 illustrates a block diagram of the experimental set-up for extracting the ESR signal. The magnetic field is generated by the field coil which receives a current from the remote-controlled power supply. By sweeping the current from the power supply in small intervals, the point at which the resonant B-field is generated can be seen from the absorption of energy recorded by the computer. This signal is provided by the Robinson oscillator as its output is sensitive to losses in energy of the tank circuit. The tank circuit lies in the centre of the field coil, and the *dpph* sample rests inside. The frequency of the oscillator is monitored by the frequency counter, and by default operates at ~50 MHz, which allows for sufficiently deep penetration into the *dpph* sample [4]. When exploring g-anisotropy in a given sample, higher frequencies are used, on the order of GHz for improved resolution, though this is beyond the scope of this investigation.

The output signal from the Robinson oscillator must be amplified since the absorption signal is very weak with low signal-to-noise ratio (SNR), as established in section 2. However, since the size of the signal is comparable to electronic noise, a simple amplifier would still output a weak ESR signal due to its indiscriminate amplification. Here, one introduces the ingenuity required to extract the ESR signal from noise, with the use of a lock-in amplifier and a modulating field, which form the remaining components in figure 3.1. An oscillating magnetic field is provided by the modulation coil, surrounding the field coil, whose frequency is set to a low audio value of 120 Hz. This value is chosen such that no other low frequency signals will interfere, such as the 50 Hz mains frequency and any harmonic of this. The mean position of the sinusoidal magnetic field is gradually swept across the absorption line by increasing the current remotely from the power supply in small increments. The peak-to-peak value of the modulation field determines the peak-to-peak change in the absorption spectrum, and will be larger for greater gradients. This method outputs the first derivative of the ESR absorption line, as illustrated in figure 3.2. The smaller the modulation amplitude, the smaller the ESR first derivative signal which is outputted, and the larger the amplitude, the less representative the output is to the

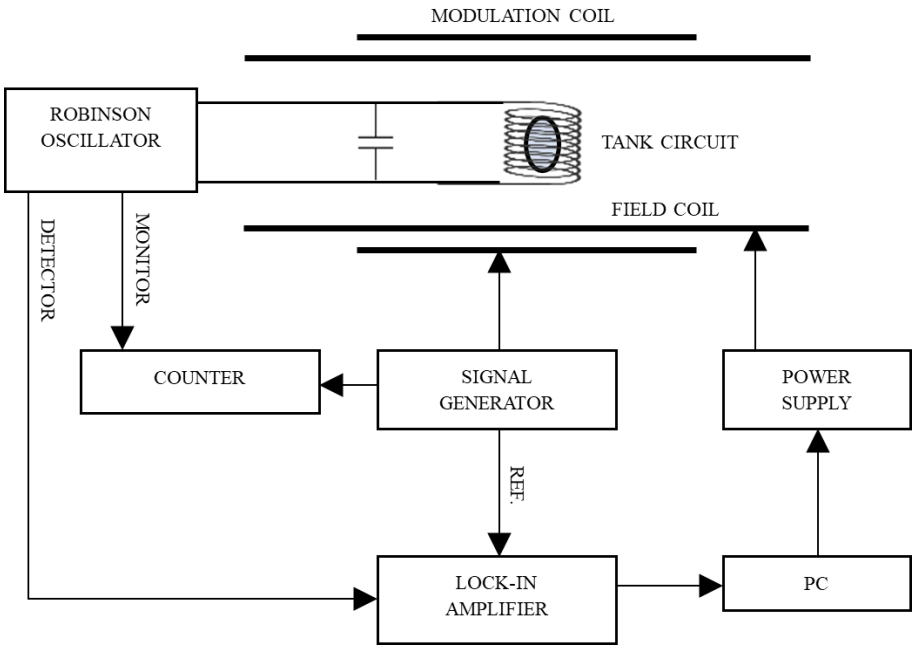

Figure 3.1: Experimental set-up for recording the ESR signal from a Robinson oscillator and tank circuit.

first derivative. First derivative spectra are preferred over true absorption spectra since they are better resolved; second derivatives have even better resolution however SNR reduces and hence a strong signal is needed [5].

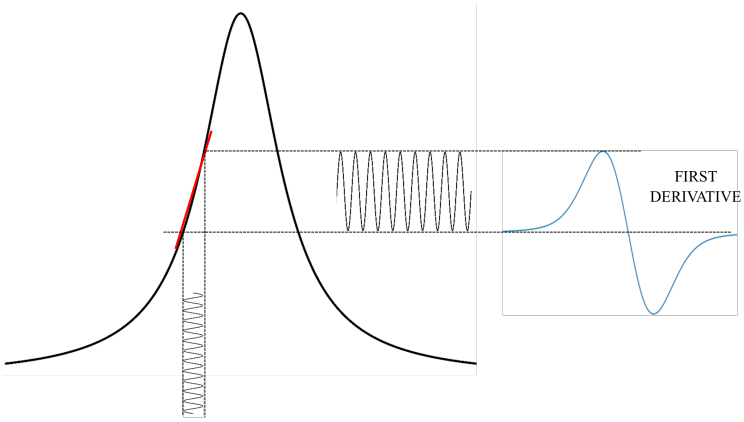

Figure 3.2: Modulating field corresponding to a sinusoidal change in absorption, from which the first derivative is extracted.

The ESR signal is amplified and isolated from noise through the lock-in amplifier, where a reference signal is set and multiplied with the input signal from the Robinson oscillator. One can model the signal from the oscillator to be a linear combination of sinusoidal functions, where one represents the desired signal, and the remaining components representing sources of noise, as illustrated by the following expression,

$$\underbrace{S\cos(\omega_s t+\phi_s)}_{\text{ESR Signal}}+\underbrace{N\cos(\omega_n t+\phi_n)}_{\text{Noise}}\,. \tag{4}$$

On multiplying this expression by a reference signal set by the lock-in amplifier with a frequency equal to that of the modulation and a phase, θ, one obtains the following signal,

$$\frac{S}{2}\{\cos(2\omega_s t+(\phi_s+\theta))+\cos(\phi_s-\theta)\}+\frac{N}{2}\{\cos((\omega_n+\omega_s)t+\phi_n+\theta)+\cos((\omega_n-\omega_s)t+\phi_n-\theta)\}. \quad (5)$$

The first term has a frequency-independent sinusoidal component that only depends on the difference in phase of the modulation signal and the reference signal. The lock-in amplifier integrates expression 5 over a time τ, the integration time, to average the signal, which attenuates any oscillatory component, leaving behind the frequency-independent term, $\frac{S}{2}cos(\phi_s - \theta)$, which is maximal when $\phi_s = \theta$. The amplitude, S, may then be determined to obtain a clean ESR signal.

4 Preliminary Investigations

4.1 Optimisation of Lock-in Amplifier Reference Phase

The change in ESR signal with reference phase of the lock-in amplifier was firstly investigated. This was performed at an arbitrary modulation amplitude since the effects of phase change and modulation amplitude are independent of each other. One would expect to see changes in the amplitude of the ESR signal as the reference phase is varied, since the signal is proportional to $\cos(\phi_s - \theta)$, as established in section 3.

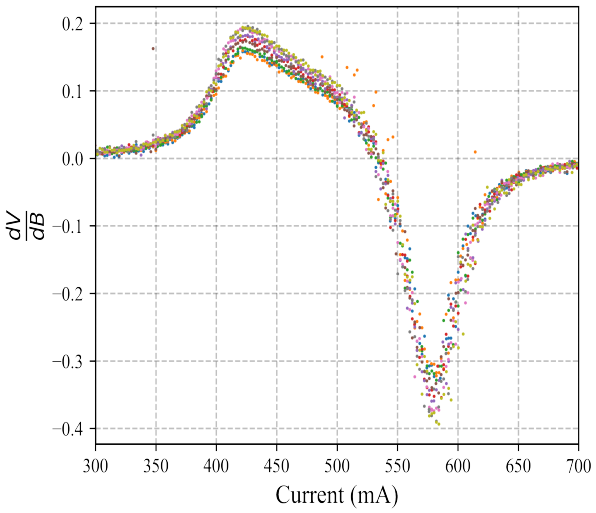

(a) Scatter ESR lines for reference phases ranging from 0° to 160°. Spread in peak values near resonance with convergence at the tails.

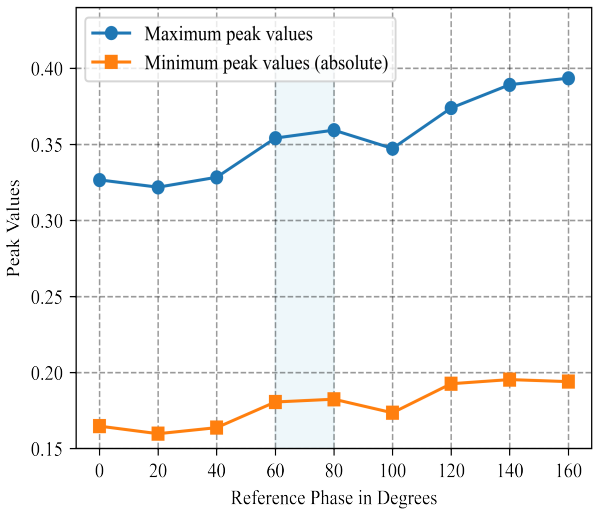

(b) Absolute values of the two ESR line peaks from figure 4.1a as a function of lock-in amplifier reference phase.

Figure 4.1: Illustration of peak variations with reference phase of lock-in amplifier.

The reference phase of the lock-in amplifier was swept from 0° to 160°, with ESR lines recorded at each 10 degree interval. Figure 4.1a illustrates the spread in peak values near resonance where changes in reference phase take a large effect. The values of the two peaks of each ESR lines were quantified, and their variation is illustrated more clearly in figure 4.1b. One sees the amplitudes reach maximum absolute values between 60 and 80 degrees, and later near 160 degrees, before reaching full circle at 180 degrees, hence its omission. The change in the two peak values are parallel up to 120 degrees, before the absolute minimum values deviate and decrease at 160 degrees, in contrast to the other peak in the ESR line. The optimal range to achieve the largest signal is therefore between 60 and 80 degrees, highlighted in blue.

The analogue dial on the lock-in amplifier was used to obtain an exact value for the desired reference phase, by obtaining the phase to achieve zero amplitude, and shifting by 90 degrees to obtain the maximum peak value in the ESR line. This was found to be -105.2 degrees, which corresponds to a reference phase of +74.8 degrees, which lies within the highlighted region of figure 4.1b. ESR lines were obtained for reference phases between -100 and -115 degrees for fine tuning, yet minimal change was seen in the peak values, hence it was decided to use -105.2 degrees as the lock-in amplifier reference phase for the largest signal.

4.2 Optimisation of Modulation Amplitude

One notes great asymmetry in the ESR lines illustrated in figure 4.1a. This was due to a relatively large peak-to-peak voltage of the modulation signal. As established in section 3, the smaller the modulation amplitude, the more accurate the first derivative line will be. Figure 4.2 illustrates the most symmetric ESR line obtained with a peak-to-peak modulation signal of 1.4 V, the lowest value possible on the signal generator. Voltages above this value rapidly led to asymmetry, as demonstrated by the shaded region which represents peak-to-peak modulation signals from 2 V to 9 V.

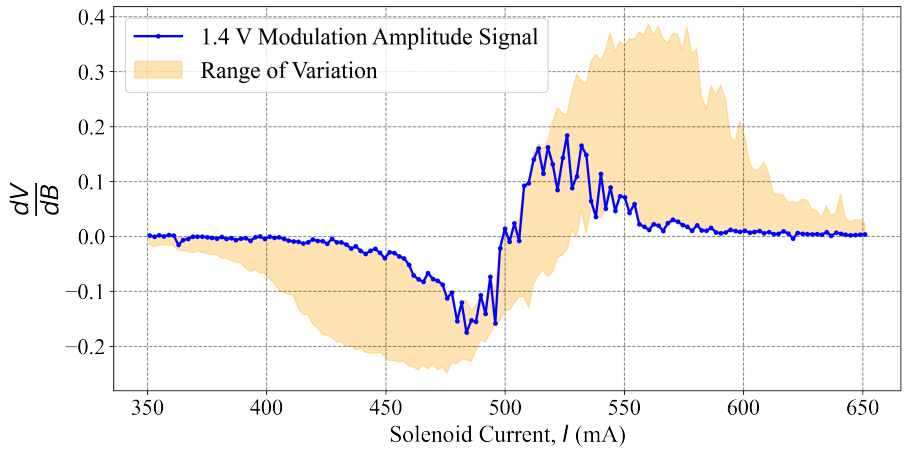

Figure 4.2: Most symmetric ESR line compared to asymmetric lines defining the shaded region.

4.3 Optimisation of Integration Time

With the optimal modulation amplitude and lock-in amplifier phase established, the integration time was subsequently increased to better attenuate noise components and obtain the clearest ESR signal. Up to this point, the time constant was set to 300 ms for rapid data acquisition. However, it was found that to attenuate noise almost completely, the integration time had to be increased substantially, since the modulation was very small. Figure 4.3 illustrates the clearest and most symmetric ESR line with a 10 second integration time.

5 Main Investigation

5.1 Determination of the *g*-factor for *dpph*

Using equation 1, one can determine the g-factor experimentally by using the resonant B-field, calculated from the resonant current obtained from the clearest ESR signal. To obtain the resonant current, I_0, a fit was needed. Noting that ESR absorption lines can take the form of Lorentzian, Gaussian, or a convolution of the two (Voigt), three fits were applied in Python [6].

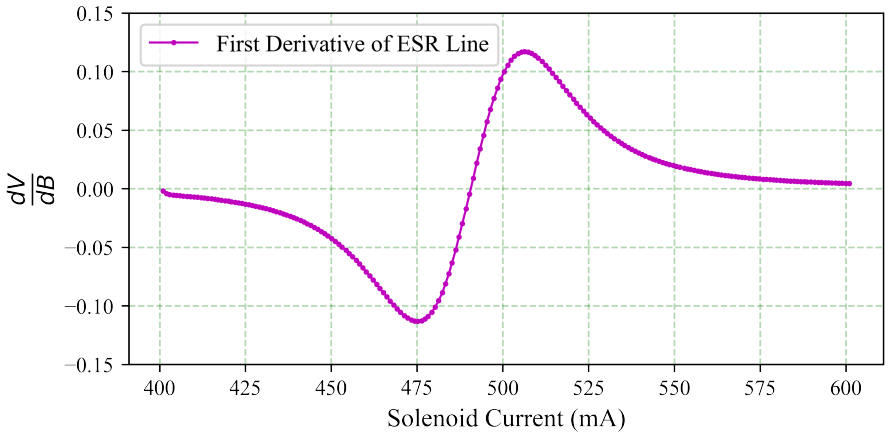

Figure 4.3: Clearest ESR first derivative line obtained with a time constant of 10 s.

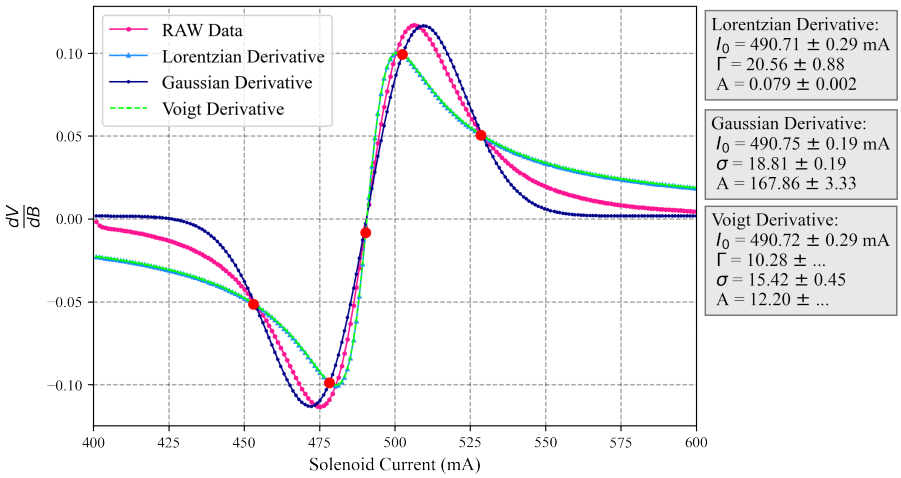

Figure 5.1: Lorentzian, Gaussian and Voigt derivatives applied as fits to the clearest ESR line. ESR first derivative line appears more Gaussian like. Voigt fit was constructed through a convolution and fitting errors could not be obtained for Γ or A.

Figure 5.1 illustrates the best-fits obtained computationally. One notes that the raw data is more Gaussian- than Lorentzian-like, and that the Voigt derivative fit is almost identical to the Lorentzian derivative fit. The similarity between the latter is likely due to a limitation of the convolution function for the best-fit, where a Lorentzian component has dominated. Despite the differences between the three, each provide I_0 with small errors, and little variation between them. Since the ESR line is more Gaussian-like, I_0 was taken to be 490.75 ± 0.19 mA. The solenoid was of length 15.2 cm and diameter 2.6 cm with 445 turns; fringe effects would be non-negligible at this scale. Accounting for this, equation 6 below was used to calculate the B-field for a given current, I, along the central axis ($r = 0$), of a solenoid of N turns, length l, diameter r_0, at a displacement z from the centre [7],

$$B_z(r=0,z) = \frac{\mu_0 N I}{2l}\left(\frac{z+l/2}{\sqrt{r_0^2+(z+l/2)^2}} - \frac{z-l/2}{\sqrt{r_0^2+(z-l/2)^2}}\right). \tag{6}$$

The B-field was calculated to be 1.708 ± 0.066 mT at the centre, yielding a g-factor of 2.091 ± 0.081. This g value is promisingly near the predicted value discussed in section 2, however is larger than the 2.0028 - 2.0036 range from literature [8][9]. The confidence interval on the experimental value does not bring the calculated g value to within the more accurate range of the literature values. There are several possibilities for this discrepancy, from a lower sensitivity

of experimental equipment, non-ideal B-field inside the coil, error on the oscillator frequency to the position of the *dpph* itself inside the tank circuit; Cohen and Kikuchi demonstrated the dependence of the g-factor on angular alignment of the sample [10].

5.2 Line width and Relaxation Time

The line width, ΔB, was obtained from the clearest spectrum (figure 4.3), by substituting ΔI into equation 6, the distance between the centroids of the minimum and maximum peaks. The current line width was found to be 31.20 mA corresponding to a line width of 0.109 $\pm$ 0.004 mT. This can be related to two types of relaxation, one where spins lose extra energy to the whole molecule (spin-lattice relaxation) and the other relating to the time constant for mutual electron spin interchange (spin-spin relaxation). In most cases, the line width is dominated by the spin-spin relaxation since this occurs over a much shorter time period than spin-lattice relaxation [3]. The spin-spin relaxation time, T_2, may be obtained from,

$$T_2 = \frac{1}{\gamma \Delta B}, \tag{7}$$

where γ is the gyromagnetic ratio. The spin-spin relaxation time of the *dpph* sample was found to be 0.050 $\pm$ 0.002 μs, which is in very close agreement to 0.053 μs relaxation time by Misra and Gupta [11].

5.3 Positional Dependence of *dpph*

The above results were obtained from placing the *dpph* sample centrally in the solenoid. Since the g-factor is a constant for a particular sample, one would expect the experimental value to remain constant regardless of location inside the solenoid. However, to meet the resonance condition, the resonant current would expect to increase being further from the centre, as the B-field is weaker, as described by equation 6, and a shift would be expected in ESR first derivative lines.

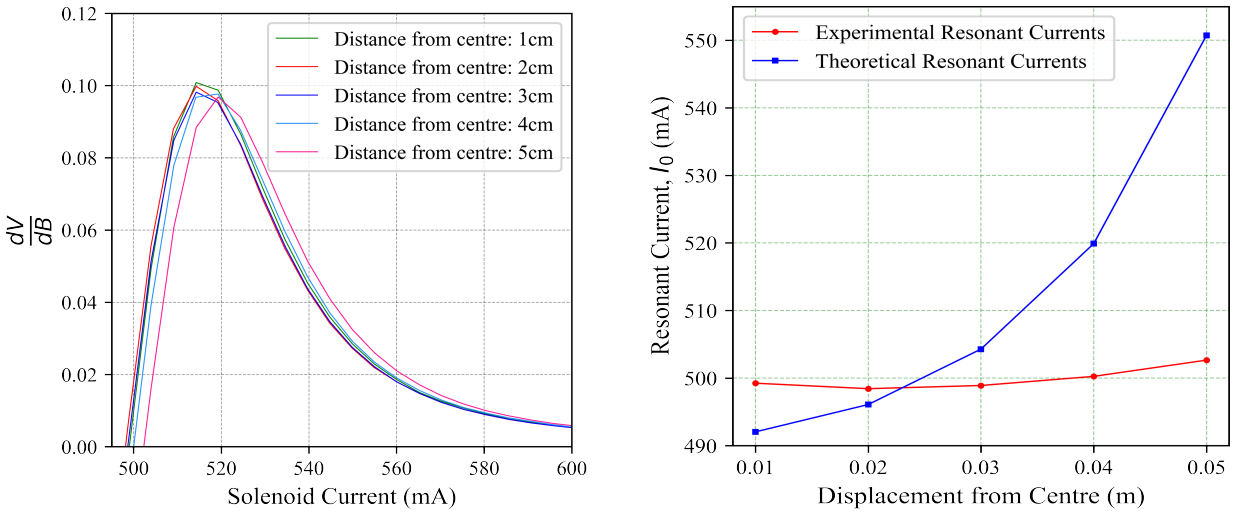

(a) ESR first derivative spectra for different *dpph* positions inside the field coil.

(b) Resonant currents obtained from fits against expected values from theory.

Figure 5.2: ESR spectra with shifts in resonant currents to compensate for weaker B-field.

Figure 5.2a illustrates a non-linear shift in I_0, with increasing shift for larger displacements. This behaviour is as expected due to the non-linear change in B-field (equation 6), where the

field begins to change more significantly at approximately 3 cm away from the centre. However, figure 5.2b illustrates that the increase in I_0 with distance of *dpph* from the centre falls short of what one would expect to maintain a constant g-factor of 2.091. The decrease at 2 cm and 3 cm is also concerning. These low resonant currents lead to vastly changing g values, as illustrated in table 1.

Table 1: I_0, g, and T_2 for increasing displacements of *dpph* from the solenoid centre.

Distance from Centre (cm)	I_0 **(mA)**	g**-factor**	T_2 (μs)
1	499.24 ± 0.42	2.061 ± 0.004	0.052 ± 0.002
2	498.42 ± 0.42	2.081 ± 0.004	0.052 ± 0.002
3	498.90 ± 0.41	2.148 ± 0.004	0.051 ± 0.002
4	500.25 ± 0.41	2.173 ± 0.004	0.045 ± 0.002
5	502.65 ± 0.42	2.291 ± 0.003	0.045 ± 0.001

This variation strongly suggests that the B-field inside the solenoid does not vary as expected from theory. Additionally, equation 6 represents the flux at the central axis; during the investigation, it is possible that the *dpph* sample was not radially central, leading to further unaccounted changes in magnetic flux. The most accurate method to obtain the resonant B-field would be to use a Hall probe placed at the position of the sample, with the resonant current fixed. Unfortunately, it was not possible to place the Hall probe perpendicular to the flux to gather accurate readings due to the confined space inside the solenoid.

The line width, ΔI, demonstrated less fluctuation, as one would expect since the ESR line shape should show little variation. Up to the point of 3 cm displacement from the centre, ΔI remained at 30.70 ± 2.00 mA, and increased to 35.70 ± 2.00 mA for 4 cm and 5 cm displacements. This sudden increase is attributed to the coarse ESR lines obtained due to fewer current points swept over; the larger error represents this. This pattern is reflected in the tabulated relaxation times, T_2, in table 1, where there is close agreement with both the experimental result in section 5.2 for small displacements, and in literature [11]. This relative consistency suggests that relaxation time does not vary with position inside the solenoid.

5.4 Frequency Dependence

A variable capacitor was added in parallel in the tank circuit, as illustrated in figure 3.1 which allows one to change the oscillation frequency from the Robinson oscillator. Since the variable capacitor was a screw mechanism between conducting rings, the frequency counter was needed to obtain accurate readings of the operating frequency. The ESR first derivative was examined at 41.5, 42.5 and 43.5 MHz. Due to time limitations, the number of current points swept over was reduced, leading to slightly more coarse lines. Additionally, the phase of the ESR signal was now different, and hence the optimal phase found in section 4.1 no longer provided the largest signal. Despite this, the peaks of the ESR signal were still prominent, as seen in figure 5.3 which allowed for fitting and line width determination, with results tabulated in table 2.

Table 2: I_0, g and T_2 for different tank circuit oscillation frequencies

Frequency (MHz)	I_0 **(mA)**	g**-factor**	T_2 (μs)
41.5	415.33 ± 0.51	2.051 ± 0.008	0.045 ± 0.001
42.5	425.39 ± 0.42	2.051 ± 0.007	0.045 ± 0.001
43.5	434.56 ± 0.53	2.055 ± 0.007	0.052 ± 0.002

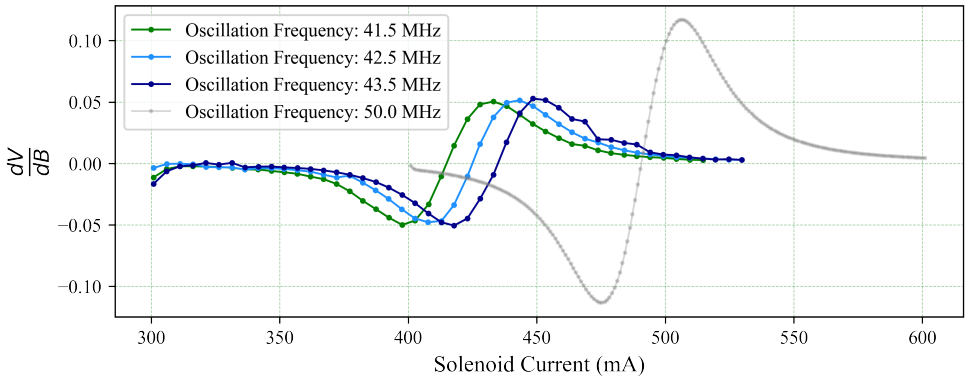

Figure 5.3: ESR first derivative lines at different tank circuit oscillation frequencies.

A linear relationship is seen between the frequency and resonant current, as expected since the resonant B-field is proportional to frequency (equation 1). The g-factor showed little fluctuation for the different microwave frequencies, which strongly suggests its independence of the tank circuit frequency. From considering the discussion above (section 5.3) on line width, and that g-factor should remain constant for a given sample, the T_2 relaxation time should remain constant. However, one notes a 7 ns discrepancy between these relaxation times at 41.5 and 42.5 MHz when compared with 43.5 MHz microwave frequency, similar to the discrepancy seen in table 1. An extended frequency range would need to be tested in order to conclude whether a lower tank circuit frequency shortens the spin-spin relaxation time, or if this is due to limited data sampling in the ESR spectra.

5.5 Temperature Dependence

Temperature effects on g-factor and line width were explored by spraying freezing agent on the *dpph* sample. The average temperature reached was approximated to 243 K, by repeating the experimental method on a digital thermometer. This is an estimated temperature where it was noted that the surface temperature was likely lower than at the centre of the sample. Despite this, one would still expect more electrons in the lower spin state from equation 3, and hence a stronger absorption signal. This is clearly observed in figure 5.4, where the magnitude of the peaks are now ~50% larger than at room temperature. The low-temperature resonant current

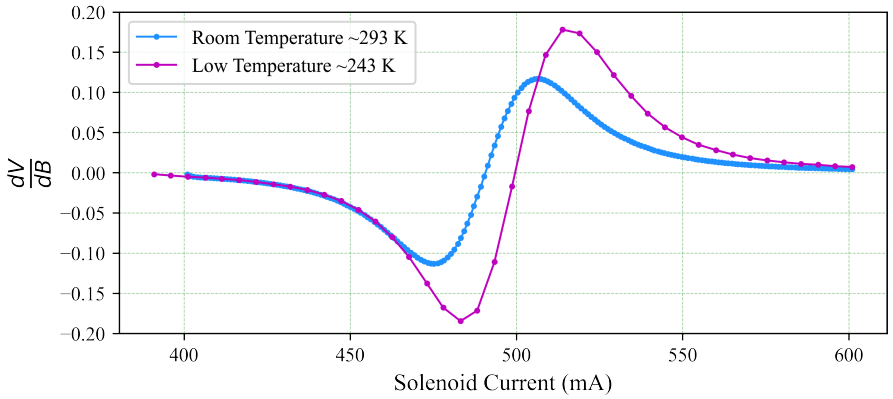

Figure 5.4: ESR first derivative lines at room temperature and low temperature, ~243 K.

was found to be 499.77 ± 0.40 mA, resulting in a B-field of 1.740 mT and a g-factor of 2.05351 ± 0.01335; only slight decrease was observed at low-temperature conditions yet non-negligible when considering the accuracy of literature values. Research by Singer and Kikuchi suggests

more obvious g-factor variations at cryogenic temperatures, attributed to the increase in g-factor anisotropy in *dpph*, which could hint at the slight variations observed in this investigation [12]. From equation 7, the spin-spin relaxation time at low temperature was calculated to be 0.034 $\pm$ 0.002 μs, shorter than any relaxation time previously calculated in this investigation. This strongly suggests a dependence of spin-spin relaxation time on temperature, as supported by Misra and Gupta who observed a reduced T_2 for lower temperatures, from 300 K to 90 K, and was true for different states of *dpph* such as powder and more recrystallised forms [11].

6 Conclusions

The g-factor for free radicals in *dpph* has been evaluated experimentally through electron spin resonance, and under the optimised parameters, was found to be 2.091 $\pm$ 0.081. This is near the accepted value from a range of literature, however is larger than hoped for when considering the accuracy of the g-factor from these papers. The respectably large error on the experimental value is attributed to the uncertainty on the magnetic field at the centre of the field coil and on the microwave frequency of the tank circuit as displayed by the counter. The investigation of positional changes of the *dpph* sample inside the field coil further illustrated the unknown behaviour of the magnetic field inside the solenoid, with resonant currents at different positions deviating drastically from theoretical predictions leading to the artificial change in experimentally determined g-factors [7]. Greater consistency was seen in this value across three different microwave frequencies of the tank circuit, where the position of the sample was held constant in the center of the field coil. This demonstrates the independence of g-factor on tank circuit frequency due to the resonant B-field changing accordingly, and further supports that irregularly changing B-field in the field coil was the likely cause for fluctuations in the factor for different positions.

The line widths of the ESR spectra were determined and related to the spin-spin relaxation time, T_2. Under the nominal conditions, this was calculated to be 0.050 $\pm$ 0.002 μs, in very close agreement with investigations by Misra and Gupta [11]. This behaved more consistent with positional changes than g-factor, yet still varied significantly at larger displacements from the coil centre, contrary to the prediction of its independence of location in a magnetic field. Similar discrepancies were also seen with changing microwave frequency of the tank circuit. The frequency sample range was limited, hence a conclusive relationship or absence of relationship between the tank circuit frequency and T_2 was not achievable. This aspect would be pursued in further study, with a wider frequency range examined.

The dependence of g-factor with temperature was not so clear due to large error margins, however from this investigation, there was a suggestion that it decreased slightly with decreased temperature, from 2.091 under nominal conditions to 2.054 at approximately 243 K. The spin-spin relaxation time demonstrated a much clearer dependence on temperature, in agreement with findings by Misra and Gupta, with shorter relaxation times for lower temperatures [11]. A clear increase in signal strength was also seen due to a larger occupancy of the lower spin states.

Further research should be focused towards line width dependence on position inside the field coil, and on tank circuit frequency, with more current points swept over, and lock-in amplifier settings optimised for cases of changing phase in ESR signal. Improvements to the experimental set-up should also be considered, such as providing sufficient space to insert a Hall probe to reach the location of the *dpph* inside the field coil. Finally, further investigation would be directed towards more formal quantification of temperature effects on g-factor and relaxation time. This would be particularly interesting for cryogenic temperatures, where unusual changes in line shape related to g-factor anisotropy are observed as seen in literature [12][13].

References

[1] Landé A. Über den anomalen zeemaneffekt (teil i). Zeitschrift für Physik. 1921;5(4):231-41.

[2] Fan X, Myers TG, Sukra BAD, Gabrielse G. Measurement of the Electron Magnetic Moment. Phys Rev Lett. 2023 Feb;130:071801. Available from: https://link.aps.org/doi/10.1103/PhysRevLett.130.071801.

[3] Ingram DJE, Moyer J. Free radicals as studied by electron spin resonance. Physics Today. 1959;12(6):42-2.

[4] Chaudhuri U, Mahendiran R. Detection of L-band electron paramagnetic resonance in the DPPH molecule using impedance measurements. RSC Adv. 2020;10:17311-6. Available from: http://dx.doi.org/10.1039/D0RA03285A.

[5] Rieger PH. Electron spin resonance: analysis and interpretation. Royal Society of Chemistry; 2007.

[6] Lund A, Shiotani M, Shimada S, Lund A, Shiotani M, Shimada S. Principles of ESR. Principles and Applications of ESR Spectroscopy. 2011:415-7.

[7] Martín-Luna P, Gimeno B, González-Iglesias D, Esperante D, Blanch C, Fuster-Martínez N, et al. On the Magnetic Field of a Finite Solenoid. IEEE Transactions on Magnetics. 2023;59(4):1-6.

[8] Valavanidis A, Iliopoulos N, Gotsis G, Fiotakis K. Persistent free radicals, heavy metals and PAHs generated in particulate soot emissions and residue ash from controlled combustion of common types of plastic. Journal of Hazardous Materials. 2008;156(1):277-84. Available from: https://www.sciencedirect.com/science/article/pii/S0304389407017694.

[9] Chaudhary A. Analysis of DPPH and $MnCl_2$ using Electron Paramagnetic Resonance (EPR) Spectroscopy. Journal of Student Research. 2022 Nov;11(4). Available from: https://www.jsr.org/hs/index.php/path/article/view/3473.

[10] Kikuchi C, Cohen VW. Paramagnetic Resonance Absorption of Carbazyl and Hydrazyl. Phys Rev. 1954 Feb;93:394-9. Available from: https://link.aps.org/doi/10.1103/PhysRev.93.394.

[11] Misra B, Gupta S. Temperature variation of relaxation time in free radical complexes. Acta Physica Academiae Scientiarum Hungaricae. 1974;37(4):347-53.

[12] Singer L, Kikuchi C. Paramagnetic resonance absorption in single crystals of diphenylpicrylhydrazyl at low temperatures. The Journal of Chemical Physics. 1955;23(9):1738-9.

[13] Fujito T. Magnetic Interaction in Solvent-free DPPH and DPPH–Solvent Complexes. Bulletin of the Chemical Society of Japan. 1981;54(10):3110-6. Available from: https://doi.org/10.1246/bcsj.54.3110.